ACS Photonics

Letter

pubs.acs.org/journal/apchd5

Efficient Collection of Light from Colloidal Quantum Dots with a Hybrid Metal–Dielectric Nanoantenna

Nitzan Livneh,[†,§] Moshe G. Harats,[‡,§] Shira Yochelis,[†] Yossi Paltiel,[†] and Ronen Rapaport*[,†,‡]

[†]The Department of Applied Physics, Selim and Rachel Benin School of Engineering and Computer Science, Jerusalem 9190401, Israel

[‡]The Racah Institute of Physics, Jerusalem 9190401, Israel

Supporting Information

ABSTRACT: We introduce a hybrid metal–dielectric nanoantenna consisting of a metallic bullseye nanostructure and a dielectric waveguide layer, for directing the photon emission of embedded colloidal nanocrystal quantum dots. This structure overcomes the intrinsic losses of plasmonic nanoantennas on one hand and is much more scalable than dielectric nanoantennas on the other. The experimental results demonstrate a very low divergence angle beam, allowing a collection efficiency of 30% of the quantum dot emission into a numerical aperture of 0.55. The experimental results are well reproduced by numerical simulations, which predict a maximal collection efficiency larger than 25% directly into a single mode fiber having a numerical aperture of 0.12 without the need for any additional optics. Such hybrid nanoantennas can significantly improve the performance of quantum dot based devices, from displays to single-photon sources.

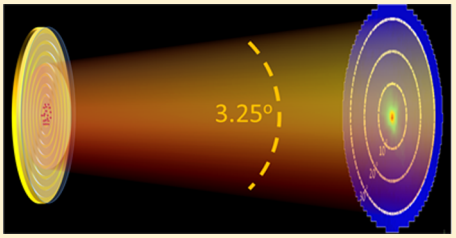

KEYWORDS: *semiconductor nanocrystals, nano-optics, nanophotonics, plasmonics, quantum dot spectroscopy, light-emitting devices*

Colloidal semiconductor nanocrystal quantum dots (NQDs) have been under the spotlight of scientific research for more than a decade as versatile sources of light. They are already used commercially for displays and show promising features for various applications ranging from lasing[1] to biological labeling[2] and quantum information,[3] where especially in the latter cases single NQDs are used as single-photon emitters. One of the problems with using NQDs as light sources is that due to their spherical or cylindrical symmetry most of the photon emission is not collected with low numerical aperture optics, so the efficiency of simple and scalable NQD-based devices is strongly reduced. This is especially limiting for practical systems requiring coupling to optical fibers.

One approach to improve the directionality and photon collection efficiency is the use of metallic nanoantennas. There are many designs for metallic nanoantennas, such as plasmonic patch antennas,[4] linear plasmonic gratings,[5] split ring resonators,[6] Yagi-Uda nanoantennas,[7] and circular (bullseye) plasmonic lenses. The bullseye geometry is a natural choice for emission pattern shaping, due to its circular symmetry, which is the desired symmetry for a beam of light for most applications.[8−10] All the structures above rely on plasmonic mode interference that directs the emission. Plasmonic modes have a low volume and higher density of states than a uniform dielectric environment, which often induce lifetime shortening of the NQDs (Purcell effect). This effect is desired since it has the potential to increase the total photon flux out of the NQDs, but it is accompanied by an increase of the probability for a nonradiative recombination.[11] This loss mechanism reduces the determinism of photon emission in plasmon-based single-photon sources, which can be detrimental for quantum technology applications. In addition, the proximity to the metal required for efficient coupling of the NQD to the plasmonic modes increases the probability for two-photon emission from the NQDs due to an increase in the biexciton emission rate. This limits their performance as pure single-photon-emitting devices.[12,13]

Another approach to improve the directionality is the use of purely dielectric nanoantennas. Such structures have been used for efficient extraction of light from light-emitting diodes,[14] where due to the high index of the host semiconductor, most of the light is emitted into the device and does not propagate out. Dielectric nanoantennas feature both high directionality and low loss.[15,16] In addition, dielectric nanoantennas can have both high quality and large Purcell factors, but this comes with a narrow frequency bandwidth, which is undesirable for room-temperature NQD emitters, as the bandwidth of even single NQDs is around 10−20 nm. Another problem with dielectric nanoantennas comes from the substantial emission into the substrate, and overcoming it requires a very demanding fabrication.[15,16]

In this work we present a hybrid metal–dielectric nanoantenna that utilizes the advantages of both metallic and dielectric nanoantennas:[5,17−20] on one hand, the NQDs can be located at a large distance from the metal and hence do not suffer from metal-related losses. On the other hand, high directionality in a broad spectral range can still be achieved by the efficient diffraction induced by the metallic bullseye

Received: August 4, 2015
Published: December 3, 2015

DOI: 10.1021/acsphotonics.5b00433
ACS Photonics 2015, 2, 1669−1674

nanostructure. With such a device we experimentally direct the emission of a few NQDs, with a very small divergence angle of only 3.25°, and show a collection efficiency larger than 30% with a numerical aperture (NA) of 0.55, which is nearly 4 times better than from free-standing NQDs.

A 3D schematic of an ideal, hybrid nanoantenna–NQD single-photon source and of a cross section of the device is depicted in Figure 1a,b, respectively. The device consists of a

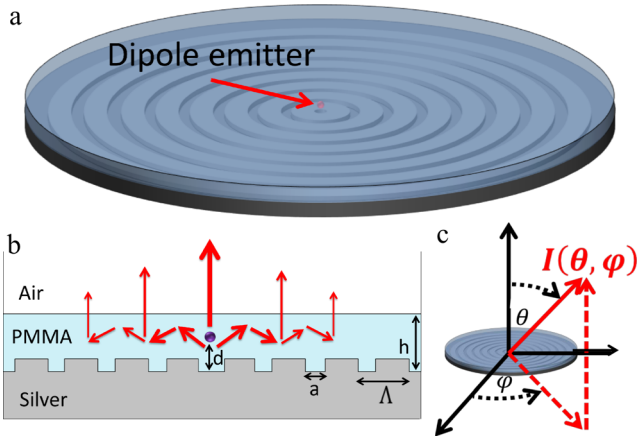

Figure 1. (a) 3D schematic drawing of the suggested hybrid metal–dielectric nanoantenna. A red sphere in the center of the structure stands for a single dipole emitter, such as an NQD. (b) Cross section of the structure, defining the geometrical parameters: period Λ, slit width a, thickness of the dielectric layer h, and height of the NQD above the surface d. The light emitted from the NQD (red arrows) is guided in the radial direction inside the dielectric layer, which acts as a slab waveguide. The periodic structure scatters the light outside of the hybrid nanoantenna to $\theta \simeq 0$. (c) The angles θ and φ are defined as the polar and azimuthal angle, respectively, measured in the far field.

low-loss metallic substrate, with a circular bullseye metallic grating and a transparent dielectric layer. A single or many NQDs are precisely positioned inside the dielectric layer, above the center of the circular grating.

The operation mechanism of the nanoantenna is schematically drawn in Figure 1b. When the NQD in the center of the device is excited, it emits the photons (having a wavelength band around a central emission wavelength, λ) preferably into the higher index dielectric layer. The dielectric layer is designed as a single-mode waveguide for this band of wavelengths, so the light propagating inside the layer has a well-defined waveguide propagation constant, β. As the light propagates in the radial direction, it is diffracted by the periodic structure. For a grating period of Λ, the grating Bragg vector $k_B = 2\pi/\Lambda$ is designed to match β, so the light is diffracted into a low-divergence beam, perpendicular to the nanoantenna surface, with a polar angle $\theta \approx 0$ (defined in Figure 1c).[5,21] The radial symmetry of the structure ensures the same grating periodicity is seen for all in-plane propagation directions of the emitted light. The prominent advantage of this design over previous plasmon-based bullseye nanoantennas[8−10] is that the lossy plasmonic modes are now replaced by low-loss waveguide modes, enabling long propagation distances along the grating, resulting in a narrower width for the diffracted beams as well as less nonradiative losses.

The efficiency of the mechanism described above strongly depends on the geometrical parameters of the nanoantenna. Therefore, an optimization of the nanoantenna geometry was first performed using a 2D Comsol simulation (see Supporting Information for details). The simulation results were in good agreement with the measurements, as will be shown later in this paper.

The sample dimensions (Figure 1b) for the simulations described in this paper are a grating period of Λ = 600 nm, slit width a = 210 nm, and dielectric layer h = 440 nm thick. The vertical distance of the NQD from the substrate d varies from one simulation to the other. The material chosen for the dielectric layer was PMMA (poly(methyl methacrylate)). It is a polymer, optically transparent around 800 nm, chemically suitable for hosting NQDs and is a standard material in current fabrication technologies.

Using the simulations we can visualize the electric fields arising from the NQD emission, in the vicinity of the hybrid nanoantenna as well as the far-field angular intensity distribution $I(\theta)$. The simulated electric field inside the structure is shown in Figure 2a. The dipole radiates into a standing waveguide mode, which is the fundamental mode of the structure. The effective wavelength inside the layer perfectly matches the period of the grating. In the air layer above the dielectric, fields propagating out of the structure are visible. The phases of these fields are set so that in the far field there is a

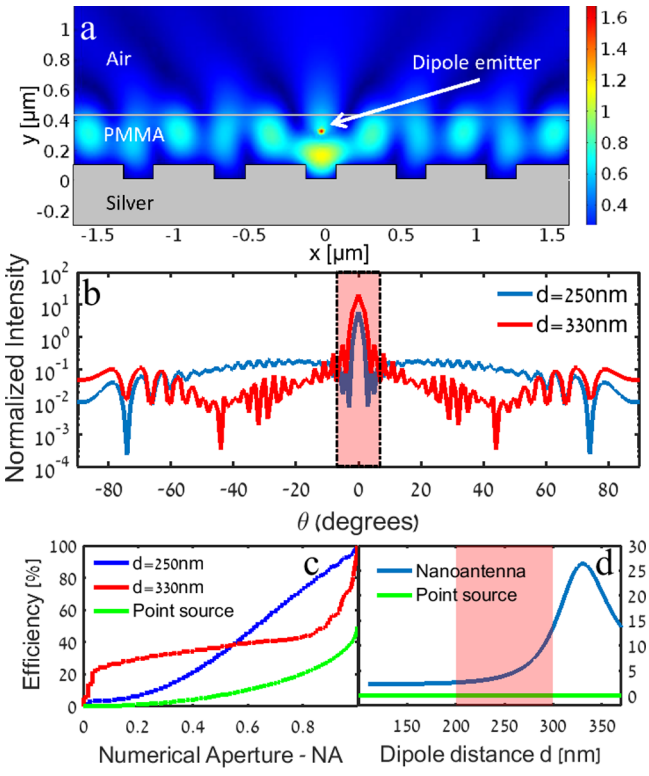

Figure 2. 2D COMSOL simulation of the hybrid nanoantenna. (a) Field distribution inside the structure. (b) Log scale normalized far-field angular intensity distribution $I(\theta)$ for d = 250 nm (blue line) and d = 330 nm (red line). The pink-shaded area corresponds to collection into NA = 0.12. (c) Calculated collection efficiency of the emission as a function of numerical aperture, for an NQD height of d = 250 nm (blue line) and d = 330 nm (red line) and for a spherically emitting point source without an antenna (green line). (d) Collection efficiency into NA = 0.12 as a function of d (blue line). The green line at 0.36% shows the collection efficiency of a spherically emitting point source without an antenna. The pink-shaded area is the location of the NQDs in the experimental hybrid nanoantenna.

DOI: 10.1021/acsphotonics.5b00433
ACS Photonics 2015, 2, 1669−1674

constructive interference to $\theta \approx 0$, the direction perpendicular to the surface. The angular intensity distribution $I(\theta)$ is plotted in Figure 2b for two values of d: 250 and 330 nm. The intensity is normalized to the total intensity into the whole space (4π). For both values of d, the intensity emitted around $\theta = 0$ is higher by at least 2 orders of magnitude compared with other angles. Since many applications require coupling the emission directly into a single mode fiber (SMF), we mark in pink in Figure 2b the numerical aperture NA = 0.12 of an SMF, which corresponds to $\theta = 6.9°$. While both values of d show strong emission into a cone defined by NA = 0.12, one can see that for $d = 250$ nm there is a nondirected emission into angles outside of the desired cone that is higher by an order of magnitude compared with the results for $d = 330$. This shows the importance of the exact vertical position of the emitter.

An important parameter quantifying the performance of the nanoantenna is the *collection efficiency* ε, defined as the intensity emitted into the collection NA, normalized to the total intensity emitted into 4π:

$$\varepsilon(\theta_{NA}) = \frac{\int_0^{\theta_{NA}} \int_0^{2\pi} I(\theta, \varphi) \sin(\theta)\, d\theta\, d\varphi}{\int_0^{\pi} \int_0^{2\pi} I(\theta, \varphi) \sin(\theta)\, d\theta\, d\varphi} \quad (1)$$

A comparison of the collection efficiencies of the emitters positioned on the nanoantenna and of a point source without a nanoantenna for $d = 250$ nm and $d = 330$ nm as a function of NA is plotted in Figure 2c. For an NQD positioned at $d = 250$ nm, 5% of the intensity is emitted into NA = 0.12, and the efficiency climbs nearly linearly for increasing NA. For $d = 330$ nm, however, 25% of the intensity is emitted into NA = 0.12, while increasing the NA increases the efficiency slowly until NA = 0.8. Surpassing NA = 0.8, the collection of the side lobes (Figure 2c) increases the efficiency to 100%. The collection efficiency of a point source without a nanoantenna is less than 0.5% for $NA = 0.12$ and increases only to 50% (as the collection is of half of the space). If the collection is into NA > 0.57, $d = 250$ nm will allow a more efficient emission collection. The simulation reveals that $d = 330$ nm is the optimal value for collection into NA = 0.12, as can be seen from the plot of the calculated collection efficiency ε as a function of d (Figure 2d). Therefore, by optimally positioning the NQD at $d = 330$ nm, an efficiency as high as 25% to emit the light directly into an SMF can be achieved. For comparison, the collection efficiency directly into an SMF from a point source with no nanoantenna is $\varepsilon = 0.36\%$ and is plotted for reference (Figure 2d).

Next we turn to fabricating a nanoantenna based on the design described above, in order to check its actual performance as compared to the simulations. A schematic cross section is depicted in Figure 3a. On top of a Ag substrate we fabricate a bullseye structure by electron beam lithography in a lift-off process, as shown in an SEM image (Figure 3b). The waveguide layer thickness is $h \approx 440$ nm, which is composed of three layers of PMMA (separated by dashed lines in Figure 3a). The bottom and top layer are made of pure PMMA, and the middle layer contains PMMA with embedded NQDs, so the NQDs are positioned in a 100 nm thick layer around $d = 250$ nm. This is not the optimal height according to the simulations, and it results from fabrication difficulties to achieve the optimal d. The sample is excited by a tightly focused (~1 μm waist) CW diode laser (405 nm) only at the center of the hybrid nanoantenna, to mimic emission from NQDs positioned only at the center.

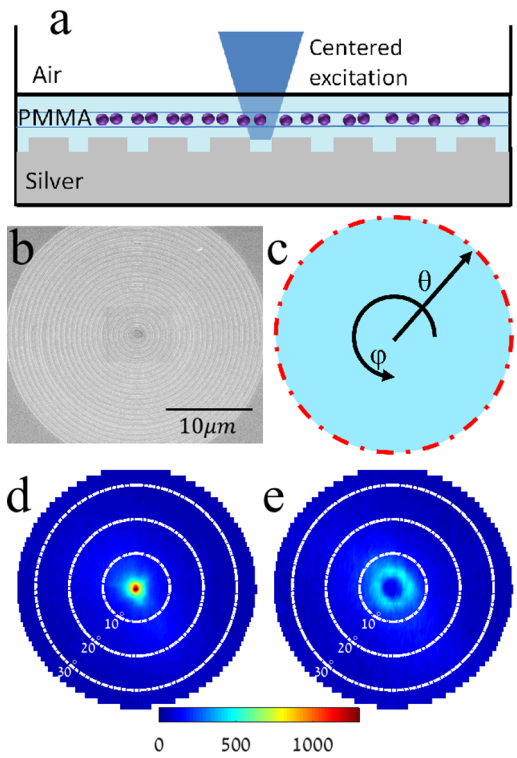

Figure 3. (a) Schematic drawing of the measured sample. The excitation is tightly focused to the center of the sample. The NQDs (schematically marked by purple circles) are embedded in a 100 nm thick layer at the center of the PMMA layer, as marked by thin blue lines. (b) SEM image of the metallic bullseye nanoantenna, fabricated by electron beam lithography. (c) A result of an angular intensity distribution $I(\theta, \varphi)$ measurement is a polar plot where the radial direction is the polar angle θ and the azimuthal angle is φ, defined in Figure 1c.[10,22] The polar plot is limited by the NA used in the experiment (dotted red circle). (d, e) Measured angular intensity distribution of the emission $I(\theta, \varphi)$ for two emission wavelengths, $\lambda = 768$ nm and $\lambda = 730$ nm, respectively. (d) Lorentzian-shaped angular intensity distribution at resonance of the structure at $\lambda = 768$ nm, with a divergence angle of 3.25°. (e) Cone-shaped angular intensity distribution off-resonance at $\lambda = 730$ nm. The color bar represents the counts normalized to the NQD emission spectrum.

The NQDs used in this experiment are Life Technologies QD800 core/shell CdTe/ZnS.[23] These NQDs have a Stokes shift between the absorption and emission spectra, so losses due to reabsorption are negligible. The NQD ensemble is spectrally broadened (~70 nm fwhm) by the size distribution of the NQDs. This gives us the opportunity to measure the emission properties from the hybrid device in a wide spectral range.

In order to map the angular intensity distribution of the NQDs, we perform a spectrally resolved measurement $I(\theta, \varphi)$ using a k-space measurement setup.[10,22] The measurement results in a 2D angular emission map defined in Figure 3c. The measured range of θ is limited by the NA of the objective lens used for light collection out of the sample. Due to the symmetry of the structure and the excitation, the angular intensity distribution at each wavelength is symmetric with respect to the azimuthal angle φ, as can be seen in Figure 3d,e.

The angular intensity distribution at 768 nm is plotted in Figure 3d. At this wavelength the emission takes the shape of a narrow directional beam, with a nearly Lorentzian profile and a divergence angle fwhm of only 3.25°. At wavelengths either

DOI: 10.1021/acsphotonics.5b00433
ACS Photonics 2015, 2, 1669−1674

longer or shorter than 768 nm the beam broadens and opens to a shape of a hollow cone, as can be seen in Figure 3e for λ = 730 nm.

Figure 4a plots the measured angular emission distribution as a function of wavelength, $I(\theta, \lambda)$, for φ = 0 (and its mirror image φ = 180°). This is compared to the simulation results (Figure 4b) with a very good agreement. The grating dispersion is clearly seen. The two diffraction orders $m = \pm 1$ meet around λ = 768 nm, to form the directional beam of Figure 3d. The two orders overlap over a range of ∼20 nm, which is compatible with the broadened line width of a room-temperature emitter. At any other wavelength the two orders of diffraction create the cone-shaped emission profile. Both the Lorentzian-shaped and the cone-shaped emission show a narrow angular broadening, as seen either from the width of the beam or from the width of each emission lobe in the cone-shaped emission. This fact is highlighted in the measured angular cross sections plotted in Figure 4c for λ = 768 nm and λ = 730 nm, respectively. The simulated angular emission for the same wavelengths are plotted in Figure 4d. The measurement results show slightly wider features than the simulation results, mostly due to the emission of NQDs positioned a bit off-center of the nanoantenna.[10] The measured divergence angle θ_d = 3.25° corresponds to a minimal spatial emission waist $2w_0 = 2\lambda/\pi\theta_d$ = 16.5 μm, which means that the emitted light propagates inside the waveguide layer for more than 13 grating cycles (26Λ in diameter) until it is diffracted out of the plane. Similar results were obtained by the simulation.

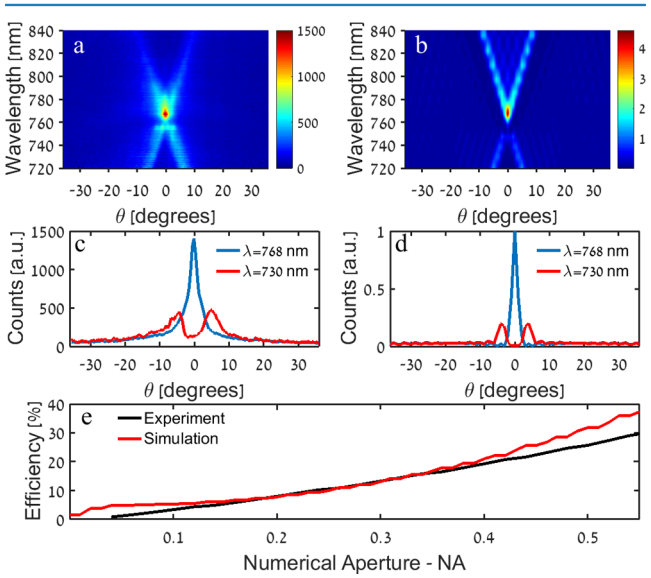

Figure 4. Experimental (a) and simulated (b) angular PL spectrum $I(\theta, \lambda)$ for φ = 0, normalized to the NQD emission spectrum, showing the dispersion curve of the device. Experimental (c) and simulated (d) angular intensity distribution $I(\theta)$ for φ = 0 at 768 nm (blue lines) and 730 nm (red lines). (e) Experimental (black) and simulated (red) emission efficiency as a function of numerical aperture for NQDs dispersed between 200 nm < d < 300 nm.

Figure 4e plots the measured (black) and simulated (red) efficiency as a function of a collection NA. The experimental plot was extracted from the angular intensity distribution measurement of Figure 3d by integrating the signal over different solid angles corresponding to different NAs. In the simulation a mean efficiency was taken for calculations of 200 nm < d < 300 nm to simulate the emission from the actual vertical position spread of the NQDs in the measured device. We see that for NA = 0.55 the collection efficiency exceeds 30%, which is nearly 4-fold better than an NQD with no antenna. Moreover, for NA = 0.12 (the NA of an SMF) we achieve an efficiency of more than 4%, which is an 11-fold enhancement with respect to an isotropic emission of an NQD with no antenna (see Figure 2c). It is important to note that the experimentally extracted efficiencies are only a lower bound, as we assumed a constant angular background at angles larger than our system's NA, while the simulations predict a decreasing background for larger angles. The reason for achieving an experimental collection efficiency of only 4% compared with the maximal calculated value of 25% is due to the imperfect vertical position spread of our NQDs. Since in our experiment the NQDs were not located in the ideal vertical position, the coupling into the correct TE waveguide mode was less than ideal. The effect of such imperfect coupling on the collection efficiency can be understood from the calculation presented in Figure 2d and in more detail in the Supporting Information: for d values smaller than 250 nm the probability for emission into the waveguide mode decreases. This is a result of an increase in emission into the competing in-plane TM polarization and to the out-of-plane polarization modes. These competing modes have broader angular dispersion and larger side lobes, and their far-field emission is therefore not well directed. This reduces the collection efficiency to a low NA = 0.12 in our device compared to the ideal case. To verify this, we calculated the expected efficiency with the experimental vertical spread of NQDs. As the NQD layer in our device is between d = 200 nm and d = 300 nm, we average the simulated efficiency into NA = 0.12 of NQDs in this vertical spread (shaded area in Figure 2d). This calculation yielded an efficiency of 5%, in agreement with the experimental results. Positioning the NQD layer at precisely d = 330 nm is predicted to enhance the efficiency for NA = 0.12 to 25%.

Another interesting point is the dip in the emission spectrum at $\lambda \simeq 750$ nm, seen in both parts a and b of Figure 4. At this wavelength the emission into the waveguide mode is suppressed. It can be explained by a Fano-resonance-like mechanism, where there is a destructive interference between the waveguide mode and the grating mode.[24]

It is illuminating to compare at this point the performance of the current hybrid design to that of previously reported directional emission using a plasmon-based bullseye nano-antenna.[10] The current hybrid metal−dielectric nanoantenna shows a reduction of more than 35% in the divergence of the NQD emission angle and an improvement of nearly 30 times in the directionality (as defined by Harats et al.[10]), but for a bandwidth slightly narrower (by 30%). It is hard to quantitatively compare the optimal efficiencies of both devices, as the nonradiative losses of plasmon-based nanoantennas strongly depend on the metal quality and roughness. The hybrid design presented here, however, is much less sensitive to these properties, which is another practical advantage.

In conclusion, we have introduced a new design for a hybrid metal−dielectric nanoantenna that directs the photon emission from colloidal NQDs over a spectral range of ∼20 nm, compatible with many modern NQD spectral spreads at room temperature, without suffering from significant losses as in plasmon-based collimators. The hybrid nanoantenna presented a very small divergence angle of only 3.25° along with a broadband high directivity and a high collection efficiency. The results are in a good agreement with the numerical simulations,

DOI: 10.1021/acsphotonics.5b00433
ACS Photonics 2015, 2, 1669−1674

supporting the physical picture of enhanced radiation into a waveguide layer and diffraction into a single diffraction order perpendicular to the nanoantenna surface. The simulations also imply that the additional background at angles beyond the collimated cone are due to positioning of the NQDs not at the ideal height above the substrate. We show that using such an antenna with a more precise vertical positioning should enable collection of more than 25% of the emitted light directly into an SMF, without the need for any additional optics, and that with simple optics having NA = 0.4 almost 40% of the photons can be collected. The hybrid nanoantenna can be further optimized to increase its efficiency by having a sinusoidal pattern, which will have less stray light diffracted out of the main order. The hybrid nanoantenna dimensions can be easily scaled to operate at every desired wavelength across the spectrum and operate with other nanoemitters, e.g, nanodiamonds.[25,26] This scalable, on-chip design can increase the efficiency of many NQD-based devices, from NQD-based displays to NQD-based single-photon sources, with the dielectric layer actively protecting the NQDs from oxidation for durability and stability of the device.

■ ASSOCIATED CONTENT

Supporting Information

The Supporting Information is available free of charge on the ACS Publications website at DOI: 10.1021/acsphotonics.5b00433.

Optimization of the nanoantenna parameters, the influence on the far-field angular intensity distribution of the different dipole orientations, the horizontal and vertical position of the dipole, the grating period and the thickness of the dielectric layer (PDF)

■ AUTHOR INFORMATION

Corresponding Author

*E-mail: ronenr@phys.huji.ac.il.

Author Contributions

§N. Livneh and M. G. Harats contributed equally to this work.

Notes

The authors declare no competing financial interest.

■ ACKNOWLEDGMENTS

This work was supported in part by the Einstein Foundation Berlin, by the U.S. Department of Energy, Office of Basic Energy Sciences, Division of Materials Science and Engineering, the European Cooperation in Science and Technology through COST Action MP1302 Nano-spectroscopy, and by the Ministry of Science and Technology, Israel.

■ REFERENCES

(1) Klimov, V. I.; Mikhailovsky, A. A.; Xu, S.; Malko, A.; Hollingsworth, J. A.; Leatherdale, C. A.; Eisler, H.-J.; Bawendi, M. G. Optical Gain and Stimulated Emission in Nanocrystal Quantum Dots. *Science* **2000**, *290*, 314−317.

(2) Dahan, M.; Laurence, T.; Pinaud, F.; Chemla, D. S.; Alivisatos, A. P.; Sauer, M.; Weiss, S. Time-gated biological imaging by use of colloidal quantum dots. *Opt. Lett.* **2001**, *26*, 825.

(3) Michler, P.; Imamoğlu, A.; Mason, M. D.; Carson, P. J.; Strouse, G. F.; Buratto, S. K. Quantum correlation among photons from a single quantum dot at room temperature. *Nature* **2000**, *406*, 968−970.

(4) Belacel, C.; Habert, B.; Bigourdan, F.; Marquier, F.; Hugonin, J.-P.; Michaelis de Vasconcellos, S.; Lafosse, X.; Coolen, L.; Schwob, C.; Javaux, C.; Dubertret, B.; Greffet, J.-J.; Senellart, P.; Maitre, A. Controlling Spontaneous Emission with Plasmonic Optical Patch Antennas. *Nano Lett.* **2013**, *13*, 1516−1521.

(5) Livneh, N.; Strauss, A.; Schwarz, I.; Rosenberg, I.; Zimran, A.; Yochelis, S.; Chen, G.; Banin, U.; Paltiel, Y.; Rapaport, R. Highly Directional Emission and Photon Beaming from Nanocrystal Quantum Dots Embedded in Metallic Nanoslit Arrays. *Nano Lett.* **2011**, *11*, 1630−1635.

(6) Hancu, I. M.; Curto, A. G.; Castro-López, M.; Kuttge, M.; van Hulst, N. F. Multipolar Interference for Directed Light Emission. *Nano Lett.* **2014**, *14*, 166−171.

(7) Curto, A. G.; Volpe, G.; Taminiau, T. H.; Kreuzer, M. P.; Quidant, R.; van Hulst, N. F. Unidirectional Emission of a Quantum Dot Coupled to a Nanoantenna. *Science* **2010**, *329*, 930−933.

(8) Jun, Y. C.; Huang, K. C. Y.; Brongersma, M. L. Plasmonic beaming and active control over fluorescent emission. *Nat. Commun.* **2011**, *2*, 283.

(9) Aouani, H.; Mahboub, O.; Bonod, N.; Devaux, E.; Popov, E.; Rigneault, H.; Ebbesen, T. W.; Wenger, J. Bright Unidirectional Fluorescence Emission of Molecules in a Nanoaperture with Plasmonic Corrugations. *Nano Lett.* **2011**, *11*, 637−644.

(10) Harats, M. G.; Livneh, N.; Zaiats, G.; Yochelis, S.; Paltiel, Y.; Lifshitz, E.; Rapaport, R. Full Spectral and Angular Characterization of Highly Directional Emission from Nanocrystal Quantum Dots Positioned on Circular Plasmonic Lenses. *Nano Lett.* **2014**, *14*, 5766−5771.

(11) Anger, P.; Bharadwaj, P.; Novotny, L. Enhancement and Quenching of Single-Molecule Fluorescence. *Phys. Rev. Lett.* **2006**, *96*, 113002.

(12) LeBlanc, S. J.; McClanahan, M. R.; Jones, M.; Moyer, P. J. Enhancement of Multiphoton Emission from Single CdSe Quantum Dots Coupled to Gold Films. *Nano Lett.* **2013**, *13*, 1662−1669.

(13) Park, Y.-S.; Ghosh, Y.; Chen, Y.; Piryatinski, A.; Xu, P.; Mack, N. H.; Wang, H.-L.; Klimov, V. I.; Hollingsworth, J. A.; Htoon, H. Super-Poissonian Statistics of Photon Emission from Single CdSe-CdS Core-Shell Nanocrystals Coupled to Metal Nanostructures. *Phys. Rev. Lett.* **2013**, *110*, 117401.

(14) Galfsky, T.; Krishnamoorthy, H. N. S.; Newman, W.; Narimanov, E. E.; Jacob, Z.; Menon, V. M. Active hyperbolic metamaterials: enhanced spontaneous emission and light extraction. *Optica* **2015**, *2*, 62−65.

(15) Davanço, M.; Rakher, M. T.; Schuh, D.; Badolato, A.; Srinivasan, K. A circular dielectric grating for vertical extraction of single quantum dot emission. *Appl. Phys. Lett.* **2011**, *99*, 041102−041102−3.

(16) Angelini, A.; Barakat, E.; Munzert, P.; Boarino, L.; De Leo, N.; Enrico, E.; Giorgis, F.; Herzig, H. P.; Pirri, C. F.; Descrovi, E. Focusing and Extraction of Light mediated by Bloch Surface Waves. *Sci. Rep.* **2014**, *4*10.1038/srep05428.

(17) Chen, X.-W.; Agio, M.; Sandoghdar, V. Metallodielectric Hybrid Antennas for Ultrastrong Enhancement of Spontaneous Emission. *Phys. Rev. Lett.* **2012**, *108*, 233001.

(18) Devilez, A.; Stout, B.; Bonod, N. Compact Metallo-Dielectric Optical Antenna for Ultra Directional and Enhanced Radiative Emission. *ACS Nano* **2010**, *4*, 3390−3396.

(19) Bigourdan, F.; Marquier, F.; Hugonin, J.-P.; Greffet, J.-J. Design of highly efficient metallo-dielectric patch antennas for single-photon emission. *Opt. Express* **2014**, *22*, 2337−2347.

(20) Badugu, R.; Szmacinski, H.; Ray, K.; Descrovi, E.; Ricciardi, S.; Zhang, D.; Chen, J.; Huo, Y.; Lakowicz, J. R. Fluorescence Spectroscopy with Metal−Dielectric Waveguides. *J. Phys. Chem. C* **2015**, *119*, 16245−16255.

(21) Schwarz, I.; Livneh, N.; Rapaport, R. General closed-form condition for enhanced transmission in subwavelength metallic gratings in both TE and TM polarizations. *Opt. Express* **2012**, *20*, 426.

(22) Tittl, A.; Harats, M. G.; Walter, R.; Yin, X.; Schäferling, M.; Liu, N.; Rapaport, R.; Giessen, H. Quantitative Angle-Resolved Small-Spot Reflectance Measurements on Plasmonic Perfect Absorbers: Impedance Matching and Disorder Effects. *ACS Nano* **2014**, *8*, 10885−10892.

DOI: 10.1021/acsphotonics.5b00433
ACS Photonics 2015, 2, 1669−1674

(23) https://www.lifetechnologies.com/order/catalog/product/Q21771MP.
(24) Miroshnichenko, A. E.; Flach, S.; Kivshar, Y. S. Fano resonances in nanoscale structures. *Rev. Mod. Phys.* **2010**, *82*, 2257−2298.
(25) Choy, J. T.; Bulu, I.; Hausmann, B. J. M.; Janitz, E.; Huang, I.-C.; Lončar, M. Spontaneous emission and collection efficiency enhancement of single emitters in diamond via plasmonic cavities and gratings. *Appl. Phys. Lett.* **2013**, *103*, 161101.
(26) Bulu, I.; Babinec, T.; Hausmann, B.; Choy, J. T.; Loncar, M. Plasmonic resonators for enhanced diamond NV- center single photon sources. *Opt. Express* **2011**, *19*, 5268.

DOI: 10.1021/acsphotonics.5b00433
ACS Photonics 2015, 2, 1669−1674